Technical University of Denmark

DTU

Voltammetry and single-molecule in situ scanning tunneling microscopy of laccases and bilirubin oxidase in electrocatalytic dioxygen reduction on Au(111) single-crystal electrodes

Climent, Victor; Zhang, Jingdong; Friis, Esben Peter; Østergaard, Lars Henrik; Ulstrup, Jens

DTU Library
Technical Information Center of Denmark

Voltammetry and Single-Molecule in Situ Scanning Tunneling Microscopy of Laccases and Bilirubin Oxidase in Electrocatalytic Dioxygen Reduction on Au(111) Single-Crystal Electrodes

Victor Climent,[†] Jingdong Zhang,[‡] Esben Peter Friis,[§] Lars Henrik Østergaard,[§] and Jens Ulstrup*[‡]

[†]Instituto de Electroquímica, Universidad de Alicante, Ap 99, E-03080 Alicante, Spain
[‡]Department of Chemistry, Building 207, Technical University of Denmark, DK-2800, Kgs Lyngby, Denmark
[§]Novozymes A/S, Krogshoejvej 36, DK-2880 Bagsværd, Denmark

Ⓢ *Supporting Information*

ABSTRACT: Laccases (E.C. 1.10.3.2) are multicopper oxidases catalytically active in the oxidation of diphenolics and related compounds by molecular dioxygen. The laccases contain a single-copper type I center and a trinuclear cluster of a single-copper type II and a dinuclear type III center. The oxidation of four equivalents of substrate near the type I copper and the sequential transfer of electrons to the trinuclear cluster are coupled with four-electron reduction of O_2 to H_2O at the latter site. Extensive efforts have been given to kinetic and structural characterization of numerous laccases to elucidate the catalytic mechanism, where laccase (sub)-monolayer voltammetry has been a core approach. In this report, we address voltammetry and electrocatalysis of O_2 reduction of (sub)monolayers of several laccases in new ways. These are based on the use of single-crystal, atomically planar bare Au(111)-electrode surfaces or surfaces modified by thiol-based self-assembled molecular monolayers. These well-defined surfaces enable introducing electrochemical scanning tunneling microscopy directly in aqueous biological media in which the enzymes are operative (in situ STM), to the level of resolution of the single enzyme molecule in electrocatalytic action. Enzyme-electrode electronic contact and intramolecular electron transfer triggered by the electrode potential or by O_2—substrate binding to the enzyme, followed at the single-molecule level, are the most important observations of this study.
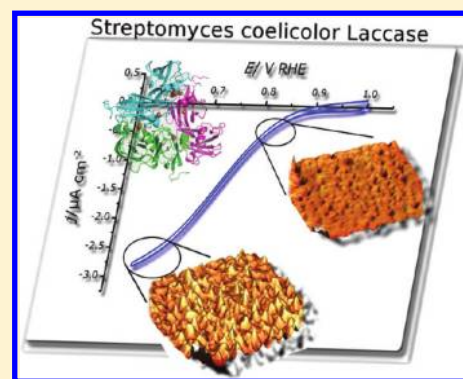
1. INTRODUCTION

Electron transfer (ET) between transition metal centers through protein "matter" is a common feature of respiratory and photosynthetic electron transport and catalysis by multi-center redox enzymes. In addition to "long-range" ET, vectorial electron transport, proton-coupled ET, conformationally fluctuating electron tunneling barriers, "gating", and "cooperative" effects are ET features in the inhomogeneous, anisotropic environment represented by the solvated protein. While understood in broad terms, biological ET continues to offer new conceptual and theoretical challenges and to be the most important molecular event in novel technology of redox enzyme catalysis. An outstanding issue is, for example, the electronic contact between the redox enzyme and a substrate molecule or an electrode surface. A common observation is that the pure enzyme shows no voltammetry, whereas strong electrocatalytic signals appear on substrate addition, indicative of electronic structural changes on substrate binding.[1−4] This is rooted in the fact that the protein structure around the active enzyme site(s) is optimized to specific electron-donating substrate molecules. Solid inorganic electrode surfaces are not natural substrates and need modification, say by self-assembled molecular monolayers (SAMs) to emulate the natural enzyme surroundings. Understandably, the

enzyme surface action is exceedingly sensitive to the nature of the SAM-promoting enzyme activity.

New technologies where biological ET processes at pure and modified electrode surfaces are in focus are encountered in areas of biosensors,[5−7] biofuel cells,[8−11] and even electrochemistry of whole bacterial cells.[12−15] Enzyme and bacterial fuel cells have been forwarded as alternatives to approaches based on expensive noble metal catalysts. Biofuel enzyme catalysts are also expensive, but this can be made up for by their selectivity and versatility. The blue multicopper oxidases and reductases offer attractive targets in all the issues noted and increasing technological interest in many areas. These range from biosensors, bioelectrocatalysis, and biofuel cells to catalysis of metabolic and energy conversion processes. They also include "pragmatic" use in haze removal in fruit juice, treatment of cork stoppers to prevent malodor, textile dye decoloring, and bleaching of paper pulp. Prompted by our recent studies of the blue copper nitrite reductase (*Achromobacter xylosoxidans*),[16−18] we address here electrochemical properties of three fungal laccases and the related bilirubin oxidase. The study is based on pure and

modified single-crystal Au(111)-electrode surfaces and on scanning tunneling microscopy directly in biological buffer solution under electrochemical potential control (in situ STM) to single-molecule structural and functional resolution.

The laccases (E.C.1.10.3.2) hold four copper ions mostly in a three-domain single enzyme molecular unit.[19−23] They operate by the "electrochemical" principle; i.e., one site, here the blue type I enzyme site, is the site of electron acceptance from external electron donors or a pure or modified electrode surface. The second site is a closely tied type II/III trinuclear copper center on which O_2 reduction is induced. The two centers are covalently connected by a His-Cys-His ligand sequence. Intramolecular ET between the type I and type II/III centers is strongly suggested by the three-dimensional laccase structures and corroborated by a wealth of thermodynamic, kinetic, and electrochemical studies.

The oxidation of four equivalents of substrate at the type I center is followed by sequential four-ET to reduce O_2 to H_2O.[24−29] Extensive efforts have been given to the structural resolution[24−29] and kinetic and electrochemical characterization with a view on disentangling the catalytic mechanisms of numerous representatives of this versatile enzyme class.[19−23,30−41] The efforts have been warranted by the ubiquity of the laccases of plant, insect, archae, bacterial, and fungal origin. To this adds the diversity of industrially interesting chemical and biological processes as noted.

The laccases offer clues to the enzyme mechanistic challenges listed. Efficient intramolecular ET between the type I and type II/III centers is almost certain to involve features of "gated" ET. In these respects, the laccases can be compared with the prototype two-center protein cytochrome c_4 for which intramolecular ET between the two heme groups is many orders faster in the immobilized state than in bulk solution.[42,43] Addition of the substrate dioxygen to immobilized laccases thus appears to open efficient ET channels between the substrate and the electrode surface through the enzyme (cf. above).[1−4,16−18,44] This feature reflects either opening of more efficient intramolecular ET channels such as for cyt c_4[43] or a substrate-induced improved electronic contact between the enzyme and the electrode surface.

The use of multicopper oxidases as electrocatalysts for O_2 reduction has been the subject of numerous studies. Apart from studies based on ET mediators,[30−33] direct ET (DET) has been achieved for this family of enzymes immobilized on different electrode surfaces. These have included graphite,[3,45−48] other carbonaceous materials,[49−51] gold,[8,38,39,48,52,53] carbon nanotubes,[34,54,55] platinum,[48,56] and gold nanoparticles.[57] In the present work, we address the catalytic activity of three laccases, *Coprinus cinereus* (CcL), *Myceliophthora thermophila* (MtL), and *Streptomyces coelicolor* laccase (ScL) as well as bilirubin oxidase from *Myrothecium verrucaria* (MvBO) in new ways. First, ScL is structurally different from the other enzymes,[24] being a trimer with approximately 3-fold symmetry. Each monomer consists of two domains, with one type I center in each domain 2 of the trimer and one trinuclear copper type II/III cluster located at each of the three interphases of adjacent monomers. Only a single study of the oxygen reduction catalysis by ScL seems to have been reported.[40] This study involved direct ET between the enzyme and a carbon nanotube modified electrode. No previous studies of the catalytic action of the other two laccases have been reported. Bilirubin oxidase is a multicopper oxidase belonging to the blue copper oxidase family. The catalysis of O_2 reduction by this enzyme has been studied several times. DET was detected in some cases,[45,46,48,49,53,54,56,57] but in other studies, mediators

were used.[30,31,52,55] DET for MvBO immobilized on gold electrodes was studied by Tominaga et al.[53] Catalytic currents were found for bare (single-crystal) gold and gold modified with different SAMs. Negatively charged SAMs ($-COOH$ and $-SO_3^-$) were found to give catalytic current, whereas SAMs terminated by $-CH_3$, $-OH$, or $-NH_2$ did not show any. A decrease of the catalytic activity with increasing length of the alkyl chain was observed for the carboxylate-terminated thiols. Gorton and associates studied bilirubin oxidase from a different organism, *Trachyderma tsunodae*.[2] They observed well-defined peaks for the enzyme covalently attached to a mercaptopropionic acid (MPA) adlayer. Recently, catalytic reduction of dioxygen by immobilized MvBO on electrodes of other materials was investigated by dos Santos et al.[48] The enzyme was immobilized on bare gold and platinum single-crystal and graphite electrodes, the latter either bare or chemically modified with naphthyl 2-carboxylate functional groups through diazonium coupling.

The present study differs from most previous studies by the use of atomically planar single-crystal pure and SAM-modified Au(111)-electrodes. These offer well-defined surfaces, the state of which can be checked by cyclic voltammetry prior to each experiment. The linker molecules were chosen to control the hydrophobic or hydrophilic nature of the surface. These features offer clues to the enzyme contact with the electrode surface, specific to the different laccases addressed. The use of atomically flat electrode surfaces enables second addressing enzyme behavior at the single-molecule level by scanning tunneling microscopy (STM). Bilewicz and associates reported STM of *Cerrena unicolor* laccase to molecular resolution,[37] but the present report offers the first study of electrochemically controlled in situ STM directly in the aqueous buffers in which the enzymes operate. This latter approach has enabled us to record both the potential dependence of the electrocatalytic action and the molecular conductivity of single enzyme molecules triggered by binding of the O_2 substrate.

2. EXPERIMENTAL SECTION

2.1. Materials. Bilirubin oxidase from *M. verrucaria* (MvBO), *Myceliophthora thermophila* laccase (MtL), *Coprinus cinereus* laccase (CcL), and *Streptomyces coelicolor* laccase (ScL) was produced at Novozymes A/S, Denmark. Enzyme solutions were diluted in 10 mM acetate buffer pH = 5.9 to ca. 2−4 mg/mL and stored frozen at −20 °C. Briefly, the genes encoding the enzymes were cloned into an expression vector using standard molecular biology techniques. After verification by DNA sequencing, the constructs were transformed into protoplasts of *Aspergillus oryzae* for expression driven by the TAKA amylase promoter. The transformed strains of *A. oryzae* were typically grown for 4 days at 37 °C in YP media with 2% maltose added. The fermentation broth was then sterile filtered to remove fungal hyphae. The resulting filtrates were used as starting material in purification of the enzymes by standard chromatographic techniques. The purified samples were stored at −20 °C until use.

Cysteamine, cysteine (both Fluka), mercaptopropionic acid (MPA) (Sigma), mercaptoundecanoic acid (MUA), 1-butanethiol, 1-octanethiol, 1-decanethiol, 1-dodecanethiol, and 1-hexadecanethiol (all from Aldrich) were used as received. Sodium acetate buffer solution of pH = 5.9 was prepared from glacial acetic acid (Sigma, 99.99+%) and sodium acetate solution (Fluka, Ultra, Biochemika) in water purified with a Millipore system (18.2 MΩ cm).

2.2. Electrodes and Instrumentation. Gold single-crystal electrodes with (111) surface orientation were prepared according to Clavilier's method as described.[58] For STM experiments, a disk electrode of 10 mm diameter (Au(111), Mateck, Germany) was used.

A glass cell with a coiled platinum wire as counter electrode and a reversible hydrogen (RHE) reference electrode located in a separate compartment connected through a Luggin Capillary were used. The RHE potential at pH 5.9 is −0.348 V vs the normal hydrogen electrode. All glassware was boiled in 15% nitric acid before use, thoroughly rinsed with Millipore water, and sonicated twice in Millipore water to remove all traces of nitric acid. All experiments were performed at room temperature (ca. 22 °C) using an Autolab electrochemical station (EcoChemie with a scangen module to produce a linear scan). Mixtures of Ar and dioxygen were prepared for the variation of dioxygen concentration using two mass flow controllers (Sierra Smart-Trak, Series 100L, Sierra Instruments).

In situ STM was performed using a Pico SPM instrument (Molecular Imaging Co., USA). Tungsten tips were electrochemically etched in 1 M KOH and insulated by Apiezon wax.[59,60] An in-house built STM cell was used accommodated in a chamber allowing control of the Ar, O_2, or air atmospheric gas.

2.3. Sample Preparation. Prior to each experiment, the electrode was electropolished and annealed in an oven. The electrode was then annealed in a hydrogen flame, cooled in a hydrogen atmosphere, and quenched in hydrogen equilibrated water.

The enzyme was attached to the electrode by spotting the surface with a drop (2−8 μL) of the enzyme solution, just after annealing in the hydrogen flame. After 2−10 min in the cell atmosphere, the electrode was rinsed with buffer solution to remove excess enzyme and then contacted with the working solution at open circuit. The open circuit potential was measured before starting the voltammetric sweep. It was always higher than 1 V (RHE) when catalytic activity was observed.

SAMs were prepared by immersing the electrode in aqueous (MPA, cysteine, and cysteamine) or ethanol (MUA and the alkylthiols) solution of the thiol (1−5 mM) overnight followed by rinsing with water or ethanol and water and then characterized by voltammetry or directly modified with the enzyme. No differences were found in the electrocatalytic behavior of the enzyme when dosed just after the thiol modification or after several voltammetric scans.

Covalent immobilization of the enzyme by amide bond formation with the carboxylate terminal groups of an MPA adlayer was also tried. After forming the SAM, the electrode was dipped into 75 mM 1-ethyl-3-(3-dimethylaminopropyl) carbodiimide (EDC) + 25 mM N-hydroxysuccinimide (NHS) solution for 30 min to activate the carboxylate groups. After rinsing with water and buffer solution, the electrode was spotted with a drop of enzyme solution as before.

3. VOLTAMMETRIC RESULTS

The surface structures of the three laccases and MvBO around the type I electrode binding site exhibit a distribution of hydrophobic patches and singly positively and negatively charged surface residues (Figure 1). The structural differences are rather subtle, and the most favorable SAM environment for a given enzyme is not immediately obvious. Similar conclusions emerged from our recent studies of Cu-nitrite reductase for which a subtle combination
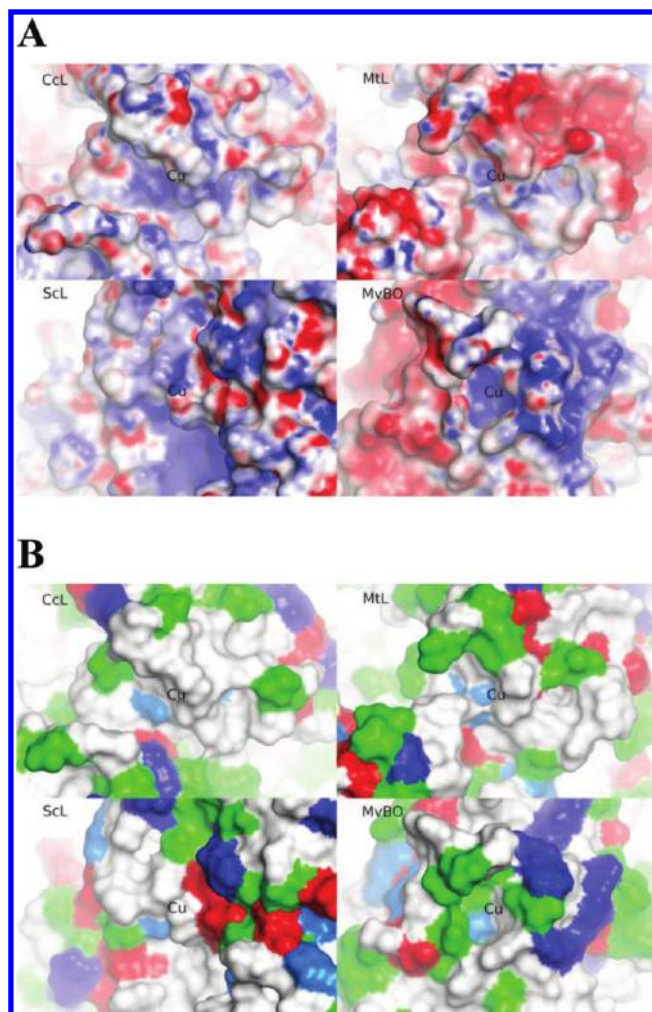

Figure 1. Graphical representation of the surface properties around the type I center for the four enzymes employed in this study, as labeled in the figure: CcL (PDB code: 1A65); MtL (homology model); ScL (PDB code: 3CG8), and MvBO (PDB code: 3ABG). The position of the type I copper ion under the surface is depicted in the center of each panel. (A) Colors according to surface potential with red = negative and blue = positive. (B) colors according to amino acid type: green = hydrophilic (Asn, Gln, Ser, Thr), red = acidic (Asp, Glu), blue = alkaline (Lys, Arg), light blue = His, white = hydrophobic (others).

of hydrophilic and hydrophobic SAMs was found to offer optimal conditions for both pure enzyme voltammetry and enzyme-catalyzed substrate (nitrite reduction) electroreduction.[16−18]

We present first voltammetric electrocatalytic data for the four enzymes at variously modified single-crystal Au(111) surfaces. Voltammetric behavior of surface-immobilized composite enzymes such as these enzymes is exceedingly sensitive to the general state of both the electrode surface and the enzymes, as illustrated.

3.1. Bilirubin Oxidase (MvBO) at Pure and Modified Single-Crystal Au(111)-Electrode Surfaces. Figure 2 summarizes electrocatalytic results of immobilized MvBO on pure Au(111) single-crystal electrodes and single-crystal Au(111)-electrodes modified by different molecular linkers. Figure 2A shows the catalytic behavior of the clean gold electrode. Significant catalytic O_2 reduction is observed. The onset of dioxygen reduction on the enzyme-modified electrode is shifted toward higher potentials by

1234

dx.doi.org/10.1021/jp2086285 |*J. Phys. Chem. C* 2012, 116, 1232–1243
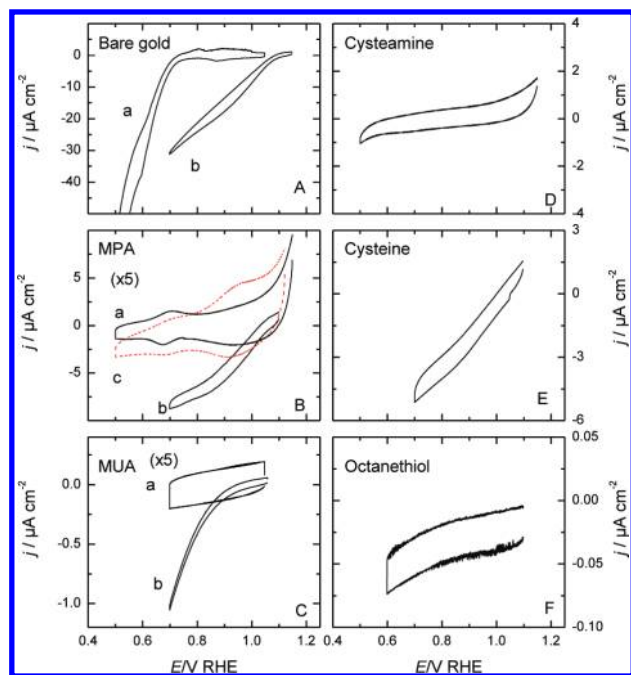
Figure 2. Cyclic voltammograms of MvBO immobilized on bare and thiol-modified Au(111)-electrodes. (A) Dioxygen reduction on bare gold electrode (a) without enzyme modification and (b) enzyme-modified electrode. (B) Enzyme immobilized onto MPA SAM. (a) Argon atmosphere. (b) Oxygen atmosphere. (c) Covalent immobilization, oxygen atmosphere. (C) Enzyme immobilized onto a MUA. (a) Argon atmosphere. (b) Oxygen atmosphere. (D) Enzyme immobilized onto a cysteamine adlayer. (E) Enzyme immobilized onto a cysteine adlayer. (F) Enzyme immobilized onto an octanethiol SAM. Sweep rate: 10 mV/s.

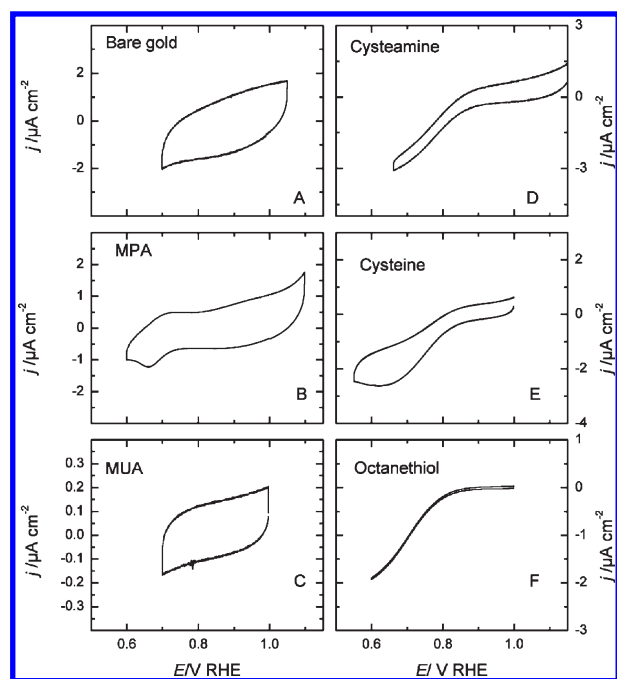**Figure 3.** Cyclic voltammograms for CcL immobilized on bare and thiol-modified electrodes. (A) Bare electrode. (B) (a) MPA, non-covalent adsorption; (b) covalent immobilization on MPA. (C) MUA. (D) Cysteamine. (E) Cysteine. (F) Octanethiol. Sweep rate: 10 mV/s. Pure oxygen atmosphere.

around 300 mV, in comparison with the bare gold electrode. This is a clear indication that the enzyme can be immobilized on the bare electrode retaining its tertiary structure in an orientation that allows electronic communication between the type I Cu center and the electrode. This observation accords with previous work[48] in which adsorption of bilirubin oxidase on different electrode materials was shown to give similar catalytic behavior.

Different SAMs terminated by methyl, carboxylate, and amino groups were tested next. Figure 2 B and C show voltammograms with the Au(111)-electrode surface modified by carboxylate-terminated SAMs with alkyl chains of 3 and 11 carbon atoms. The surface pK_a for MPA has been reported to be around 5.2−5.6.[61,62] The carboxylic units are therefore partially deprotonated at the pH of the solution, exposing a negative charge to the solution. The surface pK_a of MUA has been reported as 7.3[61] meaning that the carboxylic groups are protonated at the working pH. Voltammograms in the presence and absence of dioxygen are compared. Some catalytic current is observed in both cases although lower than when the enzyme is attached to the bare electrode. Besides, the catalytic current significantly decreases with increasing alkyl chain length. The noncatalytic currents are featureless for the enzyme adsorbed on the MUA SAM, while a clear pair of peaks is observed around 0.7 V when the enzyme is adsorbed on the MPA SAM. However, these peaks are not related to the enzyme but due to residual copper in solution from the enzyme preparation (see below). Figure 2 D and E show catalytic currents for the electrode modified with cysteamine and cysteine adlayers. Cysteamine is terminated by an amino group protonated at the working pH ($pK_a \approx 8.65$ for the immobilized
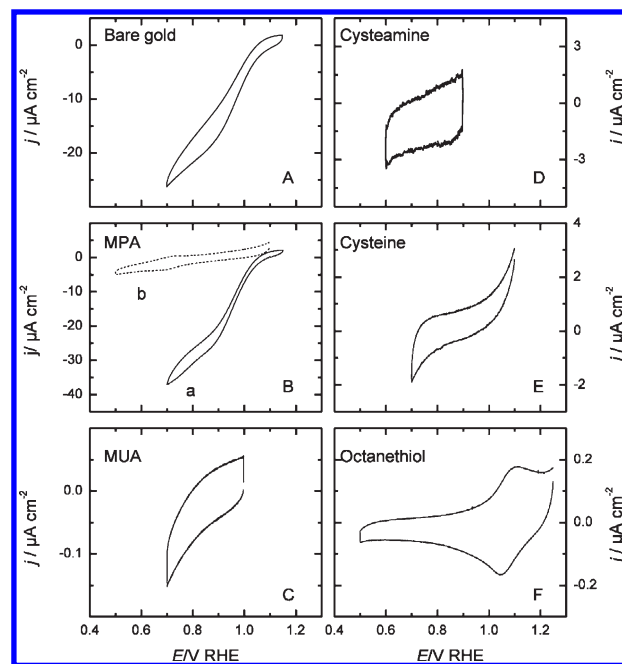
molecule[63]), creating a positively charged environment for the enzyme adsorption. The voltammogram in the presence of O_2 shows no catalytic current. Cysteine contains both carboxylate and amino groups and produces an amphoteric surface (isoelectric point of the free molecule is 5.06). Clear catalytic currents are observed in this case.

Voltammograms of MvBO attached to alkyl-terminated SAMs are illustrated in Figure 2F, with negligible catalytic current. Finally, the result of covalent immobilization of the enzyme is shown as a red line in Figure 2B. No catalytic current was observed in this case, and the CV is very similar to that for just the unactivated MPA adlayer. The small peaks around 0.7 V are also observed in this case. Additional broad peaks can be distinguished around 0.95 V. These were also observed with the MPA adlayer in some cases (not shown) depending on the number of cycles. The origin of these peaks is not clear, and they were not pursued further.

The results for MvBO demonstrate the sensitivity of the enzyme to the local environment. This sensitivity must arise from the interaction between functional groups in the amino acids around the type I center and the electrode surface. In this regard, the inactivity of the enzyme surfaces modified with SAMs terminated by hydrophobic groups suggests that the surroundings of the type I center are hydrophilic and are attracted to the carboxylic groups in MPA and MUA but not to the positively charged amino groups in the cysteamine-modified surface. Positively charged patches around the copper I center are clearly seen in Figure 1A (colored blue). Figure 1B also shows a positively charged arginine residue close to the active site, as well as other hydrophilic residues in this surface area.

3.2. *Coprinus cinereus* Laccase (CcL) and Laccase Electro-catalysis. The second target enzyme addressed, *Myceliphthora thermophila* laccase, showed no catalytic current, neither after

1235

dx.doi.org/10.1021/jp2086285 |*J. Phys. Chem. C* 2012, 116, 1232–1243

Figure 4. Cyclic voltammograms for ScL immobilized on bare and thiol-modified Au(111)-electrodes. (A) Bare electrode. (B) MPA. (C) MUA. (D) Cysteamine. (E) Cysteine. (F) Octanethiol. Sweep rate: 10 mV/s. Pure oxygen atmosphere.

Figure 5. Time evolution of the catalytic current of ScL adsorbed on the octanethiol-modified Au(111)-electrode. The arrow indicates the evolution as the time increases. Sweep rate: 10 mV/s. Pure oxygen atmosphere.

adsorption nor with covalent attachment (Figure SI1, Supporting Information). The different behavior of MvBO and MtL, in spite of their structural similarity, is likely due to a different environment around the type I center that governs the nature of the interactions between this center and the electrode surface. In this regard, MtL differs from the other enzymes in this study by its negatively charged residues around the active site.

Figure 3 shows the results for CcL. Similarly to MvBO, this enzyme shows maximum activity on bare gold. The catalytic current decays with time (Figure SI2, Supporting Information). STM data (see Supporting Information) show that the protein remains on the surface after the activity is lost. The decay is therefore rather due to protein reorientation on the surface or slow protein unfolding. The catalytic currents are much smaller on SAM-modified surfaces. A strong pair of peaks is again seen during initial cycles at 0.7 V (Figure SI3, Supporting Information) with the MPA-treated electrode, although the peaks disappeared after several cycles and a catalytic wave became apparent. These peaks are also observed after covalent immobilization of the enzyme on the MPA adlayer (dashed line in Figure 3B). Very small catalytic currents are observed also for MUA, while no catalytic current is observed with the other thiols. The observation of catalytic current with cysteine that also contains carboxylate groups is hampered by a large background current. The final notable feature is a pair of peaks around 1 V when the surface is treated with methyl-terminated SAM. The charge of these peaks is ca. 0.5 μC cm^{-2}, equivalent to a coverage around 5 pmol cm^{-2}. This value corresponds to the hexagonal packing of spheres with a diameter of 6 nm.

The 0.7 V enzyme peaks on MPA-modified electrode surfaces are observed for all four enzymes but by far the most strongly for CcL, with a charge around 50 μC cm^{-2}. This corresponds to a coverage far too large to be due to the enzyme. Besides, this
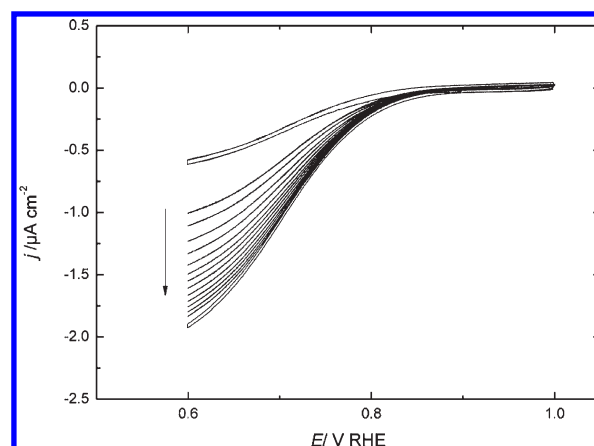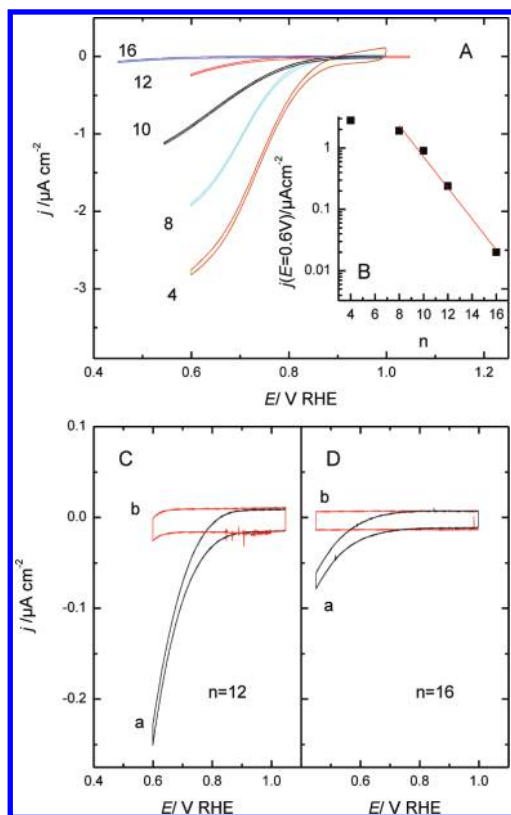
particular enzyme had been treated with excess copper to reconstitute the labile type II Cu center. To clarify the effect of copper in the enzyme solution, a blank experiment was performed by dipping the MPA-treated electrode in a CuCl$_2$ solution for two minutes, rinsing with buffer solution, transferring the electrode to the electrochemical cell, and recording the voltammogram (Figure SI4, Supporting Information). A clear pair of peaks appeared at exactly the same position as observed after immobilization of the different enzymes. This demonstrates the relation of these peaks with the Cu(I)/Cu(II) redox process and thus appears directly related to free solution copper either to maintain the coordination chemical equilibrium in the enzyme or coming from unfolded protein.

Figures 2 and 3 disclose important similarities between MvBO and CcL, most likely due to the hydrophilic functional groups around the type I Cu center. CcL is more hydrophobic that MvBO (Figure 1), although both have a positively charged area around the type I copper center.

3.3. *Streptomyces coelicolor* Laccase (ScL) Electrocatalysis. Voltammetric results for ScL are summarized in Figure 4. There are interesting differences between the behavior of ScL and the other enzymes. First, the enzyme does not show catalytic current when immobilized on the bare electrode (although a weak catalytic wave could be buried in the broad double layer charging current). Further, the carboxylate-terminated thiols that showed the higher activity for MvBO and CcL show negligible activity for ScL, whereas clear catalytic activity is observed for the amino- and alkyl-terminated SAMs. The enzyme also shows catalytic currents on the cysteine adlayer. Another difference is that the onset potential for dioxygen reduction is displaced 200 mV (to around 0.85 V) toward lower potentials in comparison with MvBO and CcL.

Octanethiol gave the clearest response, mainly due to the significantly lower double layer background current. The catalytic activity increased after each preparation of the enzyme adlayer. Figure 5 shows the time evolution of the catalytic activity where the electrode potential was cycled between 0.6 and 1.0 V over 60 cycles (ca. 80 min). During this time, the catalytic current increased from 0.6 to 1.9 μA cm^{-2}, followed by current stabilization within the time of the experiment.

The study of this enzyme was extended to variable-length alkylthiolates to investigate the effect of the SAM thickness on

1236

dx.doi.org/10.1021/jp2086285 |*J. Phys. Chem. C* 2012, 116, 1232–1243

Figure 7. Dependence of the catalytic current on the dioxygen concentration for ScL immobilized on octanethiol-modified Au(111). Sweep rate: 10 mV/s. Positive and negative sweep are averaged to remove the contribution of double layer charging. The inset shows the slow deactivation of the enzyme with time. This effect has been corrected in the curves of the main figure.
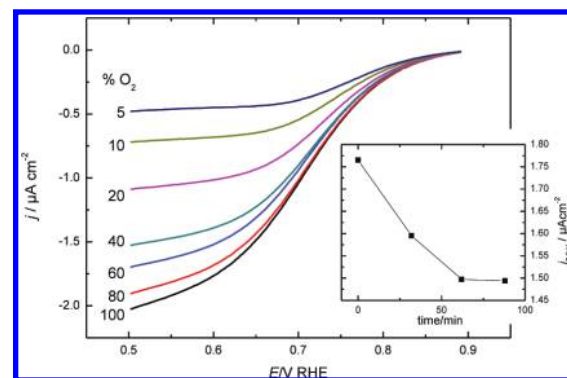
Figure 6. (A) Effect of alkyl chain length on the catalytic current for ScL on thiol-modified Au(111)-electrodes. (B) Current at 0.6 V as a function of the number of carbon atoms of the thiol modifier. (C) and D) Enlargement of the catalytic current for dodecane thiol (C) and hexadecanethiol (D). Comparison between voltammograms with (a) and without (b) enzyme. Scan rate 10 mV s^{-1}. Pure O$_2$ atmosphere.

the catalytic activity. In all cases, enough time was allowed to let the catalytic wave stabilize. The emerging stable voltammogram is shown in Figure 6. A clear decrease in the catalytic current is observed when the length of the alkyl chain is increased. Although hardly visible in the scale of Figure 6A, catalytic activity is still observed for the longer alkylthiolates used (C16 and C12). An enlargement is shown in Figure 6C and D. The voltammogram in the absence of the enzyme is included to show that the measured activity is directly related to the enzymatic catalysis. Another observation is a small displacement of the onset of dioxygen reduction toward lower potentials as well as a subtle change in voltammetric shape from sigmoidal for the shorter linkers toward a linear dependence for the longer molecules.

Figure 6B shows the dependence of the catalytic activity (measured as the current at 0.6 V) as a function of the number of carbon atoms of the thiol. Exponential decay is observed for $n \geq 8$, while saturation is reached at $n < 8$. The slope of the decay is 0.25 per carbon atom. This value is much smaller than for simple interfacial ET processes (≈ 1 per carbon atom[64,65]) reflecting the composite nature of the electrocatalytic rate constants (cf. below).

The behavior of ScL on the alkyl-terminated SAM is clearly different from that of the other enzymes and suggests a hydrophobic environment around the ScL type I center. Structural details (Figure 1) also show two negatively charged residues around the type I center. This could explain the lack of activity on surfaces modified with carboxylate-terminated thiols and the activity on the amino-terminated thiols.

3.4. Michaelis−Menten Kinetic Analysis and Variable O$_2$ Concentration.
The analysis of the effect of substrate concentration on the catalytic activity of the immobilized enzyme provides the kinetic parameters of the enzyme electrocatalytic behavior, the Michaelis constant K_M, and the maximum current, or the turnover rate j_{max}. Such analysis has been reported for bilirubin oxidase immobilized on graphite electrodes[48] and for copper nitrite reductase on variably modified Au(111) surfaces.[16,17] In view of the composite mechanism, both parameters must be denoted as "apparent" with values that depend on the potential. Such analysis was hampered in the present cases by the low stability of the immobilized enzyme. We focus on ScL on the alkyl-terminated SAM which is still stable enough to warrant analysis.

Figure 7 shows the effect of [O$_2$] variation on the catalytic current of ScL immobilized on an octanethiol-modified Au(111) electrode. To distinguish between the current decrease caused by the [O$_2$] decrease from deactivation of the enzyme with time, catalytic voltammograms with 100% oxygen atmosphere were recorded both at intermediate times and at the end of the measurements. The inset in Figure 7 shows the activity decrease caused by the slow deactivation in the presence of 100% dioxygen. This effect has been corrected in Figure 7 by the correction factor

$$\text{factor} = \frac{j_{E=0.6V, t=0}}{j_{E=0.6V, t}} \qquad (1)$$

where $j_{E=0.6V,t=0}$ is the current measured at 0.6 V in the initial voltammogram and $j_{E=0.6V,t}$ the current interpolated in the graph in the inset of Figure 7.

The Michaelis−Menten equation

$$j = \frac{j_{max}[O_2]}{K_M + [O_2]} \qquad (2)$$

was fitted to the data. [O$_2$] was calculated from the partial pressure using Henry's law and the known solubility at 298 K (1.27×10^{-3} M).[66] Figure 8A shows the Lineweaver−Burk plot, and Figure 8B a nonlinear fit of eq 2 to the data for selected potential values. Figure 8C shows corresponding values of K_M and j_{max} obtained from both plots. Both parameters show a marked dependence on the electrode potential with low values at

1237

dx.doi.org/10.1021/jp2086285 |*J. Phys. Chem. C* 2012, 116, 1232–1243
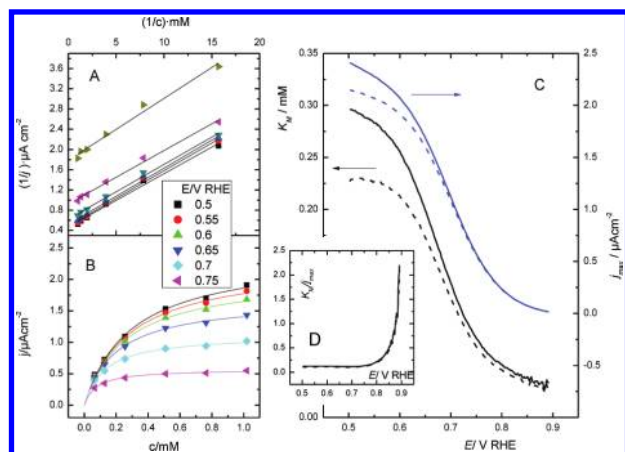
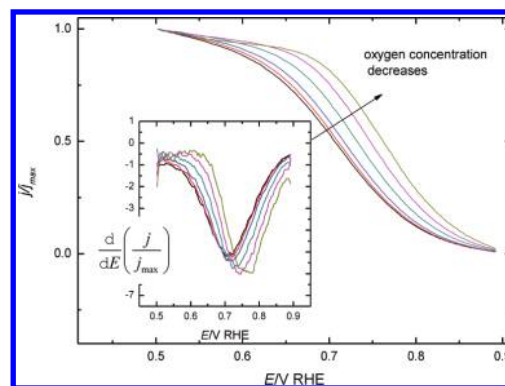**Figure 8.** Lineweaver–Burk plot (A), Michaelis–Menten plot (B), and variation of Michaelis–Menten parameters with potential (C) from the variation of the catalytic current of ScL with $[O_2]$. Dashed lines in (C) from the Lineweaver–Burk plot, solid lines from the Michaelis–Menten plot. Inset (D) shows the ratio between the two parameters.

Figure 9. Normalized currents for different dioxygen concentration in ScL electrocatalysis. Inset shows the first derivative of the curves in the main graph.

Figure 10. In situ STM images for a ScL adlayer on a butanethiol-modified Au(111)-electrode. Air atmosphere. (A) Potential 0.89 V (RHE). Bias: −0.80 V. Tunneling current: 0.035 nA. (B) Potential 0.44 V (RHE). Bias: −0.35 V. Tunneling current: 0.035 nA. 100 × 100 nm². Blue arrows mark reference points that are repeated on both images.

high potential increasing as the potential is swept toward the lower limit. Both curves level off in the low-potential limit toward an approximately constant value. The maximum K_M is around (0.27 ± 3) mM, and the maximum current density is around 2.5 $\mu A\ cm^{-2}$. The nature of the apparent Michaelis–Menten parameters, and their electrochemical potential dependence, is discussed in the Supporting Information.

The coverage of the enzyme, Γ, is needed to calculate the turnover rate. This value is not known since the nonturnover signal of the enzyme has not been detected. An upper limit would be the maximum coverage for 5–10 nm diameter spheres hexagonally packed on the surface. This would give $\Gamma = (2-8) \times 10^{-12}$ molecules cm^{-2} and a turnover rate of 1–4 s^{-1}.

In situ STM, to be addressed in Section 4, offers a unique approach to the issue of the coverage of the (single-crystal) electrode surface by *active* (as opposed to denatured) enzyme molecules on the surface. *The number* of molecular units as counted from the in situ STM images can be directly compared with the interfacial charge in the voltammetric processes. Previous studies of the blue copper electron transfer protein azurin[67] have shown that suitable electrode surface SAM modification can be brought to ascertain that close to 100% activity of immobilized metalloproteins is retained on surface immobilization.

Another observation can be extracted by scrutinizing the voltammograms at different O_2 concentrations in Figure 7. The decrease of dioxygen concentration not only decreases the peak maximum but also changes the shape of the curve which becomes steeper with a well-defined plateau at low potentials in contrast to the presence of a residual slope at higher O_2 concentration. This observation becomes more clear when the voltammogramms are normalized by the maximum current value at the lower potential limit (Figure 9). In this figure, curves obtained with a lower dioxygen concentration seem shifted to higher potentials, contrary to what would be expected from a positive reaction order toward $[O_2]$. The inset shows how the slope at the inflection point (at half wave potential) increases (in absolute value) when the dioxygen concentration is decreased. A similar result was obtained for MvBO and attributed to a change in the limiting step of the mechanism from the rate-limiting step being electron transfer
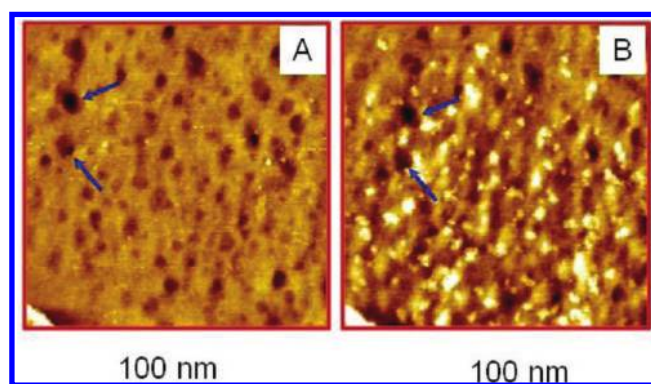
to the type 1 copper center to the intramolecular processes taking over as rate-limiting steps.[48] This explanation is framed by the model discussed below (Section 5.2). A more complete discussion of this point is given in the Supporting Information.

4. IN SITU STM OF SCL IN SINGLE-MOLECULE ENZYME ACTION AND IN THE RESTING STATE

In situ STM under electrochemical potential control offers novel clues to the enzyme activity, now at the single-molecule level. Enzyme (sub)monolayer stability is, however, essential as in situ STM experiments require relatively long preparation and data acquisition times. As noted, ScL monolayers are most robust among the four laccase-based monolayers, are stable over several hours, and were given the most attention.

In situ STM was applied to the ScL submonolayers on butanethiol-modified Au(111) surfaces. Electrochemical potentials in the voltammetrically active range were applied and the effects of substrate O_2 concentration addressed by using air, Ar, and O_2 atmosphere. Figure 10 shows in situ STM images for air atmosphere. An interesting effect of the potential on the tunneling current is observed. Figure 10 A was acquired in a potential region (0.89 V vs RHE) where the enzyme is in the oxidized state
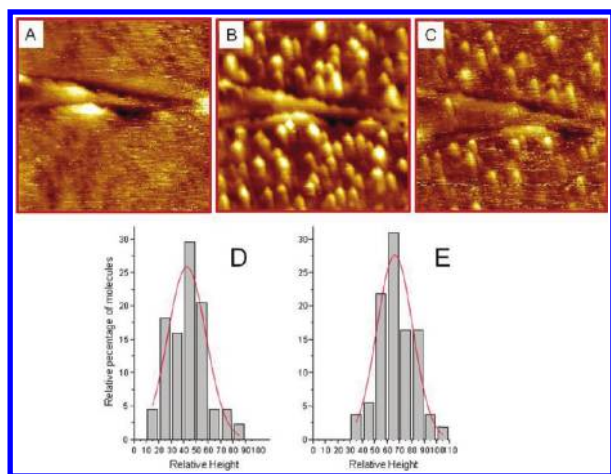
Figure 11. In situ STM images of ScL on a butanethiol-modified Au(111). Pure oxygen atmosphere. (A) Initial image at 0.84 V RHE. Bias: −0.70 V. (B) Image at 0.44 V RHE. Bias: −0.30 V. (C) Image after returning at 0.84 V RHE. Bias: −0.70 V. Tunneling current in all cases: 0.035 V. Scan area: 100×100 nm^2. (D) and (E) are histograms showing the height distribution of the bright spots in (B) and (C), respectively. Height normalization was done against the maximum height measured in (B). Lines are best fits to a normal distribution.

and no voltammetric catalytic current is observed. The images show the surface covered with dark patches (pits). Such images are characteristic of alkylthiol SAMs[60,67] and give no evidence of the presence of enzyme on the surface. The potential was then stepped negatively to 0.44 V, where the catalytic current is in the plateau region. The tip potential was kept constant giving therefore a correspondingly smaller bias voltage. Soon after the potential was decreased, bright spots started to appear on the surface (Figure 10B). This behavior was not observed when the butanethiol SAM had not been exposed to enzyme solution. The bright spots must therefore be related to the enzyme. Moreover, since there is no protein in solution, the protein coverage must remain constant. The fact that the enzyme is not observed in Figure 10A must therefore be caused by a potential-induced electronic structural change of the enzyme that opens an efficient electron tunneling channel through the enzyme and not by a change in enzyme coverage. The on–off behavior of the tunneling current is reversible, and the bright spots disappear when the potential step is reversed to the region of no catalytic current. A sequence of images where the potential was sequentially changed is shown in the Supporting Information, demonstrating the reversibility of the transformation.

In situ STM of the butanethiol/enzyme-modified surface was repeated using Ar atmosphere. Images acquired under these conditions only show the holes/pits characteristic of the SAM but no bright spots that could be assigned to tunneling through the enzyme. Some images even showed the fine structure of the ordered butanethiol adlayer (Supporting Information). When the Ar flow was stopped and air allowed into the STM chamber, the bright spots could be imaged again after a few minutes, demonstrating the relation between the presence of the O$_2$ substrate and electron tunneling of the enzyme.

The experiment was finally repeated using a pure O$_2$ atmosphere. Selected images acquired under these conditions are shown in Figure 11A–C. Similarly to the ambient air environment, the

surface shows no sign of the enzyme in electrode potential regions with no catalytic current. After decreasing the potential, bright spots appear. The spots are sharper and with a stronger in situ STM contrast than in air. As a difference from the air environment, the bright spots do not completely disappear when the potential is increased again, although the contrast significantly decreases. Figures 11D and E show histograms of the apparent height distributions of the bright spots as measured in the reduced (Figure 11B) and oxidized (Figure 11C) forms of the enzyme. This plot clearly demonstrates that the apparent average height is higher in the reduced form of the enzyme than in the oxidized form. This is most likely associated with different tunneling mechanisms which we shall discuss in the next section. Zooming out after scanning an area shows that the bright spots are concentrated in the scanned area (Supporting Information), indicative of other tip/molecule interactions in addition to electron tunneling.

5. DISCUSSION

We have studied the voltammetry and electrocatalysis of four blue multicopper oxidases, i.e., bilirubin oxidase (*M. verrucaria*) and the laccases from *M. thermofila*, *C. cinereus*, and *S. coelicolor* on variably SAM-functionalized Au(111)-electrode surfaces. The proteins displayed a variety of voltammetric behavior, reflecting the surface interactions between the proteins and the SAM-modified surfaces. In situ STM both support the voltammetric data and image the potential dependence of the enzyme in catalytic action at the level of the single molecule. We discuss first the surface protein−SAM interactions, then the voltammetric data, and finally the single-molecule redox enzyme in situ STM mapping.

5.1. Correlation between the Protein Surface Structure and the Effect of Different SAMs on the Enzyme Activity. MvBO and CcL show activity when adsorbed onto bare gold or a carboxylate-terminated SAM. In addition, MvBO showed activity on a cysteine SAM-modified electrode, probably reflecting the presence of a carboxylate group in this molecule. ScL showed no activity on the carboxylate-terminated SAMS but clear catalytic waves for alkyl- or amino-terminated SAMs. No clear catalytic current on the bare electrode was observed, although the catalytic current could be masked by the large double layer charging current of the unmodified electrode. MtL showed no activity on any of the SAMs tested.

The three-dimensional structure of MvBO has been resolved recently by X-ray crystallography.[27,28] The type I copper center is coordinated to two His and one Cys (that provides a facile ET channel to the type II/III copper atoms), as expected for a multicopper oxidase. Met is the ligand in the axial position and is probably responsible for the high redox potential of this enzyme (460 mV vs Ag/AgCl.[68]). An Asp close to the type 1 copper center has also been pointed out as an unusual environment for this center that would favor its atypical high redox potential. The structure of CcL has been resolved for the copper II depleted protein.[25] The histidines coordinating the copper atoms as well as the cysteine that provides both the characteristic absorption of the copper 1 atom and the ET channel are conserved. The axial ligand of this copper center is, however, leucine. As noted, ScL differs from the other laccases, being a trimer. Each monomer contains four copper atoms: one type 1, one type 2, and two type 3 copper atoms. Each type 1 atom binds to a single domain in each monomer, coordinated to two His and a Cys. A Met residue

Scheme 1
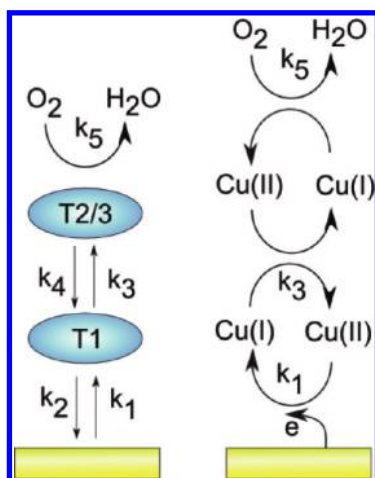
is also in contact with the type 1 copper center. The three type 1 copper atoms are located near the surface of the central part of the trimer, while each trinuclear copper cluster is located at the boundary between two monomers, coordinated to His residues from two separate protein chains. The type 1 copper and the trinuclear copper cluster are also here connected by a His-Cys-His chain.

The observed electrochemical properties can be explained by the different surface properties around the type I copper site (Figure 1). Figure 1A is colored by surface potential with red and blue areas corresponding to negative and positive patches, respectively. Figure 1B is colored according to the nature of the amino acid on the surface, where green corresponds to hydrophilic (Asn, Gln, Ser, Thr), red to acidic (Asp, Glu), and blue to alkaline amino acids (Lys, Arg). Light blue areas mark the position of His residues and white areas the hydrophobic amino acids (others).

The negative surface potential around the type 1 site for electrochemically inactive MtL (Figure 1A) is notable. It is not clear why this prevents ET via an amino-terminated SAM, but this feature is unique to MtL.

The preference for bare gold electrodes observed for CcL may be explained by the large area with electrostatic potential close to zero in the type I site region (Figure 1A). Figure 1B also shows this region as comprising hydrophobic residues only. The corresponding region of MvBO is less hydrophobic and has a positively charged surface Arg. This corresponds well with the lack of interaction with the positively charged cysteamine-modified surface.

ScL shows a less clear picture. There are two negatively charged residues close to the type I site which may explain the absence of interaction with carboxylate-terminated thiols. It is less obvious why this enzyme shows good catalytic current on an alkylthiol SAM but not on the bare gold electrode.

5.2. Electrocatalysis and Catalytic Mechanism. The mechanism for the catalytic activity of electrode-immobilized multi-copper oxidase and reductase has previously been discussed.[16,17,48] The simplified Scheme 1 offers a rationale that includes both interfacial and intramolecular ET steps. This mechanism offers a formal rationale for the observed apparent Michaelis—Menten kinetics (Figure 8), but the composite nature of the mechanism means that kinetic parameters have the character of being

"apparent". The Michaelis constant, K_M, thus depends on the potential. This reflects in turn different rate-determining steps (interfacial ET, intramolecular ET) in different potential regions. Furthermore, in the real mechanism, three electrons are sequentially transferred to form a fully reduced enzyme. O_2 binds to the reduced intermediate to form a peroxide intermediate in a two-electron oxidation process followed by a one-electron process where the oxygen—oxygen bond breaks and an oxygen radical is formed. A more detailed analysis is given in the Supporting Information.

5.3. In Situ STM. Both CcL and ScL were imaged by in situ STM to single-molecule resolution, but ScL on variable-length alkanethiol SAM-modified Au(111) showed the most stable voltammetry and electrocatalysis among the four enzymes. ScL on butanethiol SAM-modified Au(111) showing the fastest interfacial electrochemical ET was therefore chosen for detailed in situ STM. Single-molecule structural resolution in aqueous buffer was first achieved. This is notable as single-molecule in situ structural and functional STM mapping of only a few electron transfer metalloproteins[17,65,67,69−75] and even fewer large functional redox metalloenzymes have been reported.[17,18,43]

In situ STM showed, second, intriguing image pattern dependence on both the potential and the presence of dioxygen substrate. No enzyme-related structures in pure Ar atmosphere could be observed. At the same time, all the voltammetry and in situ STM data show clearly that ScL is present in high coverage on the electrode surface in the presence of oxygen. It is in fact "puzzling" and presently eludes a precise rationale that the electrode surface seems entirely electronically transparent with both underlying SAM and pits visible when the enzyme is still present in high coverage in the reduced state.

The in situ STM imaging changes entirely when the substrate dioxygen is present. No enzyme-related STM-based structures can be detected at potentials where the enzyme is catalytically inactive, i.e., in the oxidized state. Strong single-molecule, directly enzyme-related features, however, appear in potential ranges of electrocatalytic action. This effect can be oscillated reversibly between "on-" and "off-states" of potential controlled electrocatalytic action. The in situ STM images thus disclose a single-molecule "on—off" contrast pattern corresponding to the electrochemical potential control pattern with a clear distinction between the enzyme in the "resting", "off-state" and in enzyme electrocatalytic, "on-state" action, at the level of the single molecule. By their single-molecule enzyme catalysis perspectives, these observations are novel.

Previous studies have revealed at least two intermediate species in the turnover cycle.[76,77] Starting from the fully oxidized molecule, four sequential ET steps produce the fully reduced molecule, with the four copper atoms in the reduced (I) state. Binding of the O_2 molecule forms a peroxide intermediate, in which O_2 has received two electrons, from the type III center. The peroxy intermediate rapidly decays to the native fully oxidized intermediate. Although the intermediate and the resting oxidized enzyme are in the same oxidation state for all the four copper atoms, they possess important structural differences. The presence of O_2^{2-} or OH^- bridging species between the copper atoms in the trinuclear center for the native intermediate seems to facilitate rereduction of the molecule to restart the cycle.[76,77] While the rereduction of the trinuclear copper center by ET from the type I copper atom in the resting oxidized form is slow, the same process from the native intermediate is therefore much faster. It has been proposed that in this way, under turnover

conditions, the native intermediate does not decay to the resting fully oxidized form but is transformed directly to the reduced state, restarting the cycle. The key to the enhanced intramolecular ET rate is therefore the coupling of the copper atoms in the trinuclear center via the bridging oxo- or hydroxo-species that in turn trigger a more favorable driving force for the intramolecular ET steps.

The fully oxidized immobilized enzyme form with low ET rate prevails at high potentials. This is consistent with the absence of enzyme-related tunneling contrasts at these potentials. Also, in the absence of dioxygen the fully reduced molecule lacks the bridging species that enhances the intramolecular ET rate. The intramolecular ET rate is enhanced, and the enzymes can be imaged by STM only when O_2 is present and the potential is low enough to start the catalytic cycle. This conclusion is supported by a study of the intramolecular ET rate of ScL in solution.[41] Enhancement in the intramolecular ET rate in comparison with the fresh fully oxidized molecule was here observed when the enzyme is partially reduced.

Both the voltammetric data and the in situ STM single-molecule "on−off" enzyme activity patterns thus accord broadly with macroscopic laccase enzyme patterns. The combined data, however, leave questions regarding the molecular conductivity (intramolecular ET) at different electrochemical potentials and particularly electrochemical or conductivity differences in the absence and presence of dioxygen substrate. The following can be suggested. Two different single-molecule conductivity mechanisms in which triggering by dioxygen is crucial offer a rationale for the in situ STM patterns. Electron tunneling along electronic levels in the protein frame with local tunneling barrier indentations caused by the Cu centers dominate in the absence of O_2. The barrier indentations may be deep enough that Cu-based redox level population is feasible, but this is hampered by poor electronic contact at the electrode surface. Electron conduction routes therefore largely bypass the Cu centers. This mechanism accords with notions of superexchange[64,78,79] which is unfavorable due to the long tunneling distance through the protein. A similar pattern was observed for a synthetic 4-α helix heme protein.[75]

The mechanism changes drastically in the presence of dioxygen which triggers at least two effects. One effect must be a long-range effect of O_2 binding to the type II/III center through the protein to provide better electronic contact between the type I center at the opposite side and the electrode surface. This seems to be a common observation in enzyme electrochemistry where strong electrocatalytic signals are mostly without corresponding noncatalytic signals.[1,3,4,16−18,38,44,46] The other effect is associated with the prevalence of a "hopping" mechanism between the electrode and the STM tip via sequential physical population of the type I and type II/III redox centers. This mechanism follows recent theoretical efforts in framing in situ STM of large redox molecules and biomolecules.[64,65,72,78,79] Even through the individual electronic "hops", now involving attenuating nuclear reorganization, such a mechanism is strongly favored for intermediate low-lying redox levels due to the much shorter tunneling steps of the individual hops. The (close to) reversible in situ STM contrast dependence of the O_2-converting enzyme in action supports these views.

A point of notice is that the STM response to electrochemical potential changes for pure O_2 is not fully reversible. This is different both from the fully reversible in situ STM behavior in air and from the voltammetric behavior. This minor (because the contrast almost disappears on potential reversal) discrepancy

could be caused by the five times higher dioxygen concentration compared with air and the possibly slow diffusion in the confined tunneling gap. It could also be associated with the additional ET step between the enzyme and the STM tip compared with the electrochemical process.

A final "puzzle" is that the tunneling current through the enzyme seems to increase with time over the area scanned. The tip can indeed affect the protein, but previous reports[70,80] suggest that this causes the protein to desorb or denature, neither of which can be associated with more facile tunneling. A second issue is the effect of the tip on O_2 accessibility to the protein. The tip is just a few nanometers from the metal surface. This might hamper diffusion and limit the amount of dioxygen available for the catalytic cycle, but the time evolution observed must then be more complex since the protein could not be imaged in the absence of O_2. It could be conjectured that the rise of the tunneling current reflects the time dependence of the buildup of reactive intermediate oxo- and hydroxo-species that dominate the tunneling currents. This time evolution may be different in the confined tunneling gap compared with bulk solution and even have a bearing on the only partially reversible tunneling contrast behavior at high $[O_2]$ (cf. above).

As a note of conclusion, this study offers novel insight into the operation of a broad class of sophisticated multicenter redox metalloenzymes of wide technological interest. The laccases have been characterized previously in great detail, but the present study has advanced the understanding of laccase interfacial behavior by introducing multifariously modified well-defined single-crystal electrode surfaces and particularly by single-molecule in situ STM. This offers a new perspective in expanding single-molecule chemical and biological science[64,65,78,81]

■ ASSOCIATED CONTENT

ⓢ Supporting Information. Cyclic voltammograms of *Myceliphthora thermophila* laccase at bare Au(111) and Au(111) modified by MPA, MUA, cysteamine, cysteine, and octanethiol SAMs. Time evolution of the catalytic current for CcL attached to bare and MPA-modified Au(111). Cyclic voltammograms after dipping the MPA SAM-modified gold electrode into $CuCl_2$ solution. In situ STM image of *Coprinus cinereus* laccase on a bare Au(111)-electrode surface. Sequence of in situ STM images of a ScL adlayer on a buthane-modified gold electrode, acquired at different potentials. In situ STM images under argon atmosphere for ScL adsorbed on a butanethiol-modified Au(111) electrode. Analysis of voltammetric currents according to the model depicted in Scheme 1. Potential dependence of apparent Michaelis−Menten parameters. Effect of dioxygen concentration on the shape of catalytic currents. This material is available free of charge via the Internet at http://pubs.acs.org.

■ AUTHOR INFORMATION

Corresponding Author
*E-mail: ju@kemi.dtu.dk.

■ ACKNOWLEDGMENT

1241

dx.doi.org/10.1021/jp2086285 |*J. Phys. Chem. C* 2012, 116, 1232–1243

■ REFERENCES

(1) Cracknell, J. A.; Vincent, K. A.; Armstrong, F. A. *Chem. Rev.* **2008**, *108*, 2439–2461.

(2) Ramirez, P.; Mano, N.; Andreu, R.; Ruzgas, T.; Heller, A.; Gorton, L.; Shleev, S. *Biochim. Biophys. Acta, Bioenerg.* **2008**, *1777*, 1364–1369.

(3) Shleev, S.; Jarosz-Wilkolazka, A.; Khalunina, A.; Morozova, O.; Yaropolov, A.; Ruzgas, T.; Gorton, L. *Bioelectrochemistry* **2005**, *67*, 115–124.

(4) Butt, J. N.; Armstrong, F. A. In *Bioinorganic Electrochemistry*; Hammerich, O., Ulstrup, J., Eds.; Springer: Dordrecht, 2008; pp 91−128.

(5) Wilson, G. S.; Hu, Y. *Chem. Rev.* **2000**, *100*, 2693–2704.

(6) *Electrochemistry of Nucleic Acids and Proteins − Towards Electrochemical Sensors for Genomics and Proteomics*; Paleček, E., Scheller, F., Wang, J., Eds.; Elsevier: Amsterdam, 2005.

(7) Zhang, X.; Ju, H.; Wang, J. *Electrochemical Sensors, Biosensors and their Applications*; Academic Press: San Diego, 2008.

(8) Barton, S. C.; Gallaway, J.; Atanassov, P. *Chem. Rev.* **2004**, *104*, 4867–4886.

(9) Heller, A. *Phys. Chem. Chem. Phys.* **2004**, *6*, 209–216.

(10) Moehlenbrock, M. J.; Minteer, S. D. *Chem. Soc. Rev.* **2008**, *37*, 1188–1196.

(11) Willner, I.; Yan, Y. M.; Willner, B.; Tel-Vered, R. *Fuel Cells* **2009**, *9*, 7–24.

(12) Schroder, U. *Phys. Chem. Chem. Phys.* **2007**, *9*, 2619–2629.

(13) Coman, V.; Gustavsson, T.; Finkelsteinas, A.; von Wachenfeldt, C.; Hagerhall, C.; Gorton, L. *J. Am. Chem. Soc.* **2009**, *131*, 16171–16176.

(14) Debabov, V. G. *Microbiology* **2008**, *77*, 123–131.

(15) Logan, B. E.; Hamelers, B.; Rozendal, R.; Schroder, U.; Keller, J.; Freguia, S.; Aelterman, P.; Verstraete, W.; Rabaey, K. *Environ. Sci. Technol.* **2006**, *40*, 5181–5192.

(16) Welinder, A. C.; Zhang, J.; Hansen, A. G.; Moth-Poulsen, K.; Christensen, H. E. M.; Kuznetsov, A. M.; Bjornholm, T.; Ulstrup, J. *Z. Phys. Chem.* **2007**, *221*, 1343–1378.

(17) Zhang, J. D.; Welinder, A. C.; Hansen, A. G.; Christensen, H. E. M.; Ulstrup, J. *J. Phys. Chem. B* **2003**, *107*, 12480–12484.

(18) Chi, Q. J.; Zhang, J. D.; Jensen, P. S.; Christensen, H. E. M.; Ulstrup, J. *Faraday Discuss.* **2006**, *131*, 181–195.

(19) Solomon, E. I.; Sundaram, U. M.; Machonkin, T. E. *Chem. Rev.* **1996**, *96*, 2563–2606.

(20) Sakurai, T.; Kataoka, K. *Chem. Rec.* **2007**, *7*, 220–229.

(21) Blanford, C. F.; Heath, R. S.; Armstrong, F. A. *Chem. Commun.* **2007**, 1710–1712.

(22) Rodgers, C. J.; Blanford, C. F.; Giddens, S. R.; Skamnioti, P.; Armstrong, F. A.; Gurr, S. J. *Trends Biotechnol.* **2010**, *28*, 63–72.

(23) Davies, G. J.; Ducros, V. In *Handbook of Metalloproteins*; Messerschmidt, A., Huber, R., Poulos, T., Wieghardt, K., Eds.; Wiley: Chichester, 2001; pp 1359−1368.

(24) Skalova, T.; Dohnalek, J.; Ostergaard, L. H.; Osteryaard, P. R.; Kolenko, P.; Duskova, J.; Stepankova, A.; Hasek, J. *J. Mol. Biol.* **2009**, *385*, 1165–1178.

(25) Ducros, V.; Brzozowski, A. M.; Wilson, K. S.; Ostergaard, P.; Schneider, P.; Svendson, A.; Davies, G. J. *Acta Crystallogr., Sect. D: Biol. Crystallogr.* **2001**, *57*, 333–336.

(26) Ducros, V.; Brzozowski, A. M.; Wilson, K. S.; Brown, S. H.; Ostergaard, P.; Schneider, P.; Yaver, D. S.; Pedersen, A. H.; Davies, G. J. *Nat. Struct. Biol.* **1998**, *5*, 310–316.

(27) Cracknell, J. A.; McNamara, T. P.; Lowe, E. D.; Blanford, C. F. *Dalton Trans.* **2011**, *40*, 6668–6675.

(28) Mizutani, K.; Toyoda, M.; Sagara, K.; Takahashi, N.; Sato, A.; Kamitaka, Y.; Tsujimura, S.; Nakanishi, Y.; Sugiura, T.; Yamaguchi, S.; Kano, K.; Mikami, B. *Acta Crystallogr., Sect. F: Struct. Biol. Cryst. Commun.* **2010**, *66*, 765–770.

(29) Hakulinen, N.; Kiiskinen, L. L.; Kruus, K.; Saloheimo, M.; Paananen, A.; Koivula, A.; Rouvinen, J. *Nat. Struct. Biol.* **2002**, *9*, 601–605.

(30) Mano, N.; Fernandez, J. L.; Kim, Y.; Shin, W.; Bard, A. J.; Heller, A. *J. Am. Chem. Soc.* **2003**, *125*, 15290–15291.

(31) Dronov, R.; Kurth, D. G.; Moehwald, H.; Scheller, F. W.; Lisdat, F. *Angew. Chem., Int. Ed.* **2008**, *47*, 3000–3003.

(32) Palmore, G. T. R.; Kim, H. H. *J. Electroanal. Chem.* **1999**, *464*, 110–117.

(33) Fernandez-Sanchez, C.; Tzanov, T.; Gubitz, G. M.; Cavaco-Paulo, A. *Bioelectrochemistry* **2002**, *58*, 149–156.

(34) Zheng, W.; Li, Q. F.; Su, L.; Yan, Y. M.; Zhang, J.; Mao, L. Q. *Electroanalysis* **2006**, *18*, 587–594.

(35) Tsujimura, S.; Kamitaka, Y.; Kano, K. *Fuel Cells* **2007**, *7*, 463–469.

(36) Stolarczyk, K.; Nazaruk, E.; Rogalski, J.; Bilewicz, R. *Electrochim. Acta* **2008**, *53*, 3983–3990.

(37) Klis, M.; Maicka, E.; Michota, A.; Bukowska, J.; Sek, S.; Rogalski, J.; Bilewicz, R. *Electrochim. Acta* **2007**, *52*, 5591–5598.

(38) Pita, M.; Shleev, S.; Ruzgas, T.; Fernandez, V. M.; Yaropolov, A. I.; Gorton, L. *Electrochem. Commun.* **2006**, *8*, 747–753.

(39) Shleev, S.; Christenson, A.; Serezhenkov, V.; Burbaev, D.; Yaropolov, A.; Gorton, L.; Ruzgas, T. *Biochem. J.* **2005**, *385*, 745–754.

(40) Gallaway, J.; Wheeldon, I.; Rincon, R.; Atanassov, P.; Banta, S.; Barton, S. C. *Biosens. Bioelectron.* **2008**, *23*, 1229–1235.

(41) Farver, O.; Tepper, A. W.; Wherland, S.; Canters, G. W.; Pecht, I. *J. Am. Chem. Soc.* **2009**, *131*, 18226–18227.

(42) Raffalt, A. C.; Schmidt, L.; Christensen, H. E. M.; Chi, Q.; Ulstrup, J. *J. Inorg. Biochem.* **2009**, *103*, 717–722.

(43) Chi, Q. J.; Zhang, J. D.; Arslan, T.; Borg, L.; Pedersen, G. W.; Christensen, H. E. M.; Nazmudtinov, R. R.; Ulstrup, J. *J. Phys. Chem. B* **2010**, *114*, 5617–5624.

(44) Willner, B.; Willner, I. In *Bioinorganic Electrochemistry*; Hammerich, O., Ulstrup, J., Eds.; Springer: Dordrecht, 2008; pp 37−90.

(45) Tsujimura, S.; Nakagawa, T.; Kano, K.; Ikeda, T. *Electrochemistry* **2004**, *72*, 437–439.

(46) Shleev, S.; El Kasmi, A.; Ruzgas, T.; Gorton, L. *Electrochem. Commun.* **2004**, *6*, 934–939.

(47) Miura, Y.; Tsujimura, S.; Kamitaka, Y.; Kurose, S.; Kataoka, K.; Sakurai, T.; Kano, K. *Chem. Lett.* **2007**, *36*, 132–133.

(48) dos Santos, L.; Climent, V.; Blanford, C. F.; Armstrong, F. A. *Phys. Chem. Chem. Phys.* **2010**, *12*, 13962–13974.

(49) Nogala, W.; Celebanska, A.; Szot, K.; Wittstock, G.; Opallo, M. *Electrochim. Acta* **2010**, *55*, 5719–5724.

(50) Miura, Y.; Tsujimura, S.; Kurose, S.; Kamitaka, Y.; Kataoka, K.; Sakurai, T.; Kano, K. *Fuel Cells* **2009**, *9*, 70–78.

(51) Tsujimura, S.; Miura, Y.; Kano, K. *Electrochim. Acta* **2008**, *53*, 5716–5720.

(52) Dronov, R.; Kurth, D. G.; Scheller, F. W.; Lisdat, F. *Electroanalysis* **2007**, *19*, 1642–1646.

(53) Tominaga, M.; Ohtani, M.; Taniguchi, I. *Phys. Chem. Chem. Phys.* **2008**, *10*, 6928–6934.

(54) Weigel, M. C.; Tritscher, E.; Lisdat, F. *Electrochem. Commun.* **2007**, *9*, 689–693.

(55) Gobel, G.; Lisdat, F. *Electrochem. Commun.* **2008**, *10*, 1691–1694.

(56) Yan, Y. M.; Baravik, I.; Tel-Vered, R.; Willner, I. *Adv. Mater.* **2009**, *21*, 4275–4279.

(57) Murata, K.; Kajiya, K.; Nakamura, N.; Ohno, H. *Energy Environ. Sci.* **2009**, *2*, 1280–1285.

(58) Hamelin, A. *J. Electroanal. Chem.* **1996**, *407*, 1–11.

(59) Chi, Q. J.; Zhang, J. D.; Nielsen, J. U.; Friis, E. P.; Chorkendorff, I.; Canters, G. W.; Andersen, J. E. T.; Ulstrup, J. *J. Am. Chem. Soc.* **2000**, *122*, 4047–4055.

(60) Zhang, J. D.; Chi, Q. J.; Ulstrup, J. *Langmuir* **2006**, *22*, 6203–6213.

(61) Zhao, J. W.; Luo, L. Q.; Yang, X. R.; Wang, E. K.; Dong, S. J. *Electroanalysis* **1999**, *11*, 1108–1111.

(62) Dai, Z.; Ju, H. X. *Phys. Chem. Chem. Phys.* **2001**, *3*, 3769–3773.

(63) Molinero, V.; Calvo, E. J. *J. Electroanal. Chem.* **1998**, *445*, 17–25.

(64) Zhang, J.; Chi, Q.; Kuznetsov, A. M.; Hansen, A. G.; Wackerbarth, H.; Christensen, H. E. M.; Andersen, J. E. T.; Ulstrup, J. *J. Phys. Chem. B* **2002**, *106*, 1131–1152.

(65) Zhang, J.; Kuznetsov, A. M.; Medvedev, I. G.; Chi, Q.; Albrecht, T.; Jensen, P. S.; Ulstrup, J. *Chem. Rev.* **2008**, *108*, 2737–2791.

(66) Lide, D. R.; Frederiksen, H. P. R. *CRC handbook of chemistry and physics*; CRC Press: Boca Raton, 1998.

(67) Chi, Q. J.; Farver, O.; Ulstrup, J. *Proc. Natl. Acad. Sci. U.S.A.* **2005**, *102*, 16203–16208.

(68) Kamitaka, Y.; Tsujimura, S.; Kataoka, K.; Sakurai, T.; Ikeda, T.; Kano, K. *J. Electroanal. Chem.* **2007**, *601*, 119–124.

(69) Alessandrini, A.; Corni, S.; Facci, P. *Phys. Chem. Chem. Phys.* **2006**, *8*, 4383–4397.

(70) Hansen, A. G.; Boisen, A.; Nielsen, J. U.; Wackerbarth, H.; Chorkendorff, I.; Andersen, J. E. T.; Zhang, J. D.; Ulstrup, J. *Langmuir* **2003**, *19*, 3419–3427.

(71) Zhang, J. D.; Christensen, H. E. M.; Ooi, B. L.; Ulstrup, J. *Langmuir* **2004**, *20*, 10200–10207.

(72) Della Pia, E. A.; Chi, Q. J.; Jones, D. D.; Macdonald, J. E.; Ulstrup, J.; Elliott, M. *Nano Lett.* **2011**, *11*, 176–182.

(73) Welinder, A. C.; Zhang, J. D.; Steensgaard, D. B.; Ulstrup, J. *Phys. Chem. Chem. Phys.* **2010**, *12*, 9999–10011.

(74) Gwyer, J. D.; Zhang, J. D.; Butt, J. N.; Ulstrup, J. *Biophys. J.* **2006**, *91*, 3897–3906.

(75) Albrecht, T.; Li, W. W.; Ulstrup, J.; Haehnel, W.; Hildebrandt, P. *ChemPhysChem* **2005**, *6*, 961–970.

(76) Lee, S. K.; George, S. D.; Antholine, W. E.; Hedman, B.; Hodgson, K. O.; Solomon, E. I. *J. Am. Chem. Soc.* **2002**, *124*, 6180–6193.

(77) Solomon, E. I.; Augustine, A. J.; Yoon, J. *Dalton Trans.* **2008**, 3921–3932.

(78) Zhang, J.; Albrecht, T.; Chi, Q.; Kuznetsov, A. M.; Ulstrup, J. In *Bioinorganic Electrochemistry*; Hammerich, O., Ulstrup, J., Eds.; Springer: Dordrecht, 2008.

(79) Kuznetsov, A. M.; Ulstrup, J. *J. Phys. Chem. A* **2000**, *104*, 11531–11540.

(80) Zhang, J. D.; Kuznetsov, A. M.; Ulstrup, J. *J. Electroanal. Chem.* **2003**, *541*, 133–146.

(81) Zhang, J.; Chi, Q.; Jensen, P. S.; Ulstrup, J. In *Frontiers in Bioelectrochemistry*; Alkire, R. C., Kolb, D. M., Lipkowski, J., Eds.; Wiley-VCH: New York, 2011.